arXiv:1612.06540v1 [astro-ph.HE] 20 Dec 2016

Magnetic fields in turbulent quark matter and magnetar bursts

Maxim Dvornikov[a,b*]

[a] Pushkov Institute of Terrestrial Magnetism, Ionosphere and Radiowave Propagation (IZMIRAN), 108840 Troitsk, Moscow, Russia;

[b] Physics Faculty, National Research Tomsk State University, 36 Lenin Avenue, 634050 Tomsk, Russia

Abstract

We analyze the magnetic field evolution in dense quark matter with unbroken chiral symmetry. In our study we take into account the chiral magnetic effect, the electroweak interaction between quarks, and the turbulent motion of quark matter. The evolution equations for the spectra of the magnetic helicity density and the magnetic energy density as well as for the chiral imbalances are obtained. On the basis of the numerical solution of these equations, we find that turbulence effects are important for the behavior of relatively small scale magnetic fields. It is revealed that, under certain initial conditions, the time evolution of the magnetic field resembles the electromagnetic flashes of some magnetars. We suggest that these magnetic fields, created inside a magnetized compact star, can initiate magnetar bursts.

1 Introduction

The emission of the strong electromagnetic radiation by some astrophysical objects called anomalous X-ray pulsars (AXP) and soft γ-ray repeaters (SGR) is likely to be associated with the transformation of the magnetic energy in the star interiors to the energy of hard photons [1]. The estimates of the internal magnetic field strength necessary to explain the observed flashes give the value $B \gtrsim 10^{15}\,\mathrm{G}$, making these compact stars one of the most powerful magnets in the universe, or magnetars [1]. Despite the existence of the numerous models for the generation of such strong magnetic fields based on classical magnetohydrodynamics, this issue is still an open problem for the modern astrophysics. Note that the

*maxdvo@izmiran.ru

actual mechanism for the transfer of the internal magnetic energy to the stellar magnetosphere is unclear either. Some of the popular models for the description of magnetars are reviewed in Ref. [1].

Recently several attempts to explain the processes happening in magnetars with help of the elementary particles methods were undertaken. For example, the chiral magnetic effect (CME) [2], which leads to the magnetic field instability resulting in the enhancement of a seed field, potentially can be used for the explanation of magnetic fields in magnetars. Note that CME can be also involved to account for the high linear velocities of pulsars [3]. These astrophysical applications of CME are reviewed in Ref. [4].

Recently, in Ref. [5], we proposed the new model for the generation of strong magnetic fields in magnetars based on the magnetic field instability driven by the parity violating electroweak interaction between background fermions. In this model the contribution of the electroweak interaction was a correction to CME. Note that the idea about the magnetic field instability induced by the parity violating interaction was put forward earlier in Ref. [6].

Then, in Ref. [7], the similar idea about the magnetic field amplification driven by the electroweak interaction was implemented in dense quark matter in a hybrid star (HS) or in a quark star (QS). Sometimes QS is also called a strange star because of the presence of the s quark component. Although these compact stars have not been observed yet, there is a quite strong theoretical motivation for their existence [8].

In this work we continue the study of the magnetic field evolution in dense quark matter where the chiral symmetry is restored and, thus, both CME and the electroweak correction can take place. Since the typical time for the magnetic field growth found in Ref. [7] appeared to be much shorter than that in Ref. [5], the magnetic field amplification can happen in earlier stages of the stellar evolution when the effects of the turbulent motion of stellar matter are sizable. Thus the main motivation of the present work will be the study of the magnetic field evolution accounting for both CME, and the electroweak interaction between quarks, and the effects of the matter turbulence. Recently analogous problem in the early universe plasma was studied in Ref. [9].

The present paper is organized as follows. In Sec. 2, we derive the main equations describing the evolution of the magnetic field in frames of our model. These evolution equations are solved numerically in Sec. 3. The results of the numerical simulations are applied in Sec. 4 to explain the electromagnetic radiation of magnetars. In Sec. 5 we summarize our results. The calculation of the drag time in dense quark matter is given in Appendix A.

2 Model for the magnetic field evolution in dense quark matter

In this section we shall establish the system of the evolution equations for the spectra of the magnetic helicity density $h(k,t)$ and the magnetic energy density $\rho_{\rm B}(k,t)$ as well as

of the chiral imbalances of u and d quarks $\mu_{5(u,d)}$. This system will take into account the effects of the turbulent matter motion.

Let us consider a degenerate quark matter consisting of u and d quarks. We shall assume that the matter density is high enough for the chiral symmetry to be restored. In this case CME can happen in this system. In Ref. [7], accounting for the electroweak interaction between quarks, we showed that the anomalous electric current $\mathbf{J}_5$ along the external magnetic field $\mathbf{B}$ is induced in this matter,

$$\mathbf{J}_5 = \Pi \mathbf{B}, \quad \Pi = \frac{1}{2\pi^2} \sum_{q=u,d} e_q^2 \left(\mu_{5q} + V_{5q}\right), \tag{1}$$

where $e_u = 2e/3$ and $e_d = -e/3$ are the electric charges of quarks, $e > 0$ is the elementary charge, $\mu_{5q} = \left(\mu_{q\mathrm{R}} - \mu_{q\mathrm{L}}\right)/2$ is the chiral imbalance, $\mu_{q\mathrm{R,L}}$ are the chemical potentials of right and left quarks, $V_{5q} = \left(V_{q\mathrm{L}} - V_{q\mathrm{R}}\right)/2$, and $V_{q\mathrm{L,R}}$ are the effective potentials of the electroweak interaction of left and right quarks with background fermions [10]. If we suppose that the quark matter is electrically neutral, one gets that $V_{5u} = 0.28 G_{\mathrm{F}} n_0$ and $V_{5d} = 0.18 G_{\mathrm{F}} n_0$, where $G_{\mathrm{F}} = 1.17 \times 10^{-5}\,\mathrm{GeV}^{-2}$ is the Fermi constant, $n_0 = n_u + n_d$ is the total number density of quarks, and $n_{u,d}$ are the number densities of u and d quarks. If we take that $n_0 = 1.8 \times 10^{38}\,\mathrm{cm}^{-3}$, which corresponds to the typical quark matter in HS/QS, we get that $V_{5u} = 4.5\,\mathrm{eV}$ and $V_{5u} = 2.9\,\mathrm{eV}$ [7].

We shall describe the evolution of the magnetic field in an isotropic matter using the magnetic helicity density h and the magnetic energy density ρ_{B}, which are defined as

$$h(t) = \frac{1}{V} \int \mathrm{d}^3 x \left(\mathbf{A} \cdot \mathbf{B}\right), \quad \rho_{\mathrm{B}}(t) = \frac{1}{2V} \int \mathrm{d}^3 x B^2, \tag{2}$$

where $\mathbf{A}$ is the vector potential of the magnetic field and V is the normalization volume. It is convenient to express $h(t)$ and $\rho_{\mathrm{B}}(t)$ in terms of their spectral representations $h(k,t)$ and $\rho_{\mathrm{B}}(k,t)$ in the form,

$$h(t) = \int \mathrm{d}k h(k,t), \quad \rho_{\mathrm{B}}(t) = \int \mathrm{d}k \rho_{\mathrm{B}}(k,t), \tag{3}$$

where the integration is over all the range of the wave number k variation.

In Ref. [9], we studied the evolution of the magnetic field in the relativistic electron fluid accounting for the chiral magnetic effect and the turbulence. The effects of the turbulence were simulated by the replacement of the fluid velocity $\mathbf{v}$, obeying the Navier-Stokes equation, with the Lorentz force [11]:

$$\mathbf{v} = \frac{\tau_{\mathrm{D}}}{\rho_{\mathrm{E}} + p} \left(\mathbf{J} \times \mathbf{B}\right), \tag{4}$$

where ρ_{E} is the energy density of the fluid, p is the pressure, $\mathbf{J}$ is the total electric current, and τ_{D} is the drag time, which is a phenomenological parameter meaning the typical Coulomb collision time in plasma [12]. The computation of τ_{D} in the degenerate quark

matter is given in Appendix A (see Eq. (30) for the final result). If we study the degenerate relativistic quark gas, then $p = \rho_{\rm E}/3$, $\rho_{\rm E} = \left(\mu_u^4 + \mu_d^4\right)/4\pi^2 = 2 \times 10^{-2}\mu_0^4$, $\mu_q = \left(3\pi^2 n_q\right)^{1/3}$ is the mean chemical potential of each quark component, and $\mu_0 = \left(3\pi^2 n_0\right)^{1/3} = 346\,\mathrm{MeV}$.

Generalizing the results of Ref. [9] by considering the chiral imbalances of u and d quarks and including the nonzero effective potentials V_{5q}, we get the following system of the evolution equations for $h(k,t)$, $\rho_{\rm B}(k,t)$, and μ_{5u}:

$$
\begin{aligned}
\frac{\partial h(k,t)}{\partial t} =& -2k^2\left[\frac{F_q^{5/6}}{\sigma_{\rm cond}} + \frac{4}{3}\frac{\tau_{\rm D}}{\rho_{\rm E}+p}\int \mathrm{d}k'\rho_{\rm B}(k',t)\right] h(k,t) \\
&+ 4\left[\frac{2\alpha_{\rm em}F_q^{5/6}}{\pi\sigma_{\rm cond}}\left\{\frac{4}{9}\left[\mu_{5u}(t)+V_{5u}\right] + \frac{1}{9}\left[\mu_{5d}(t)+V_{5d}\right]\right\}\right. \\
&\left.+ \frac{2}{3}\frac{\tau_{\rm D}}{\rho_{\rm E}+p}\int \mathrm{d}k'k'^2 h(k',t)\right]\rho_{\rm B}(k,t), \\
\frac{\partial \rho_{\rm B}(k,t)}{\partial t} =& -2k^2\left[\frac{F_q^{5/6}}{\sigma_{\rm cond}} + \frac{4}{3}\frac{\tau_{\rm D}}{\rho_{\rm E}+p}\int \mathrm{d}k'\rho_{\rm B}(k',t)\right] \rho_{\rm B}(k,t) \\
&+ \left[\frac{2\alpha_{\rm em}F_q^{5/6}}{\pi\sigma_{\rm cond}}\left\{\frac{4}{9}\left[\mu_{5u}(t)+V_{5u}\right] + \frac{1}{9}\left[\mu_{5d}(t)+V_{5d}\right]\right\}\right. \\
&\left.- \frac{2}{3}\frac{\tau_{\rm D}}{\rho_{\rm E}+p}\int \mathrm{d}k'k'^2 h(k',t)\right]k^2 h(k,t), \\
\frac{\mathrm{d}\mu_{5u}(t)}{\mathrm{d}t} =& \frac{\pi\alpha_{\rm em}F_q^{5/6}}{\mu_u^2\sigma_{\rm cond}}\frac{4}{9}\int \mathrm{d}k\left[k^2 h(k,t)\right. \\
&\left.- \frac{4\alpha_{\rm em}}{\pi}\left\{\frac{4}{9}\left[\mu_{5u}(t)+V_{5u}\right] + \frac{1}{9}\left[\mu_{5d}(t)+V_{5d}\right]\right\}\rho_{\rm B}(k,t)\right] - \Gamma_u\mu_{5u}(t), \\
\frac{\mathrm{d}\mu_{5d}(t)}{\mathrm{d}t} =& \frac{\pi\alpha_{\rm em}F_q^{5/6}}{\mu_d^2\sigma_{\rm cond}}\frac{1}{9}\int \mathrm{d}k\left[k^2 h(k,t)\right. \\
&\left.- \frac{4\alpha_{\rm em}}{\pi}\left\{\frac{4}{9}\left[\mu_{5u}(t)+V_{5u}\right] + \frac{1}{9}\left[\mu_{5d}(t)+V_{5d}\right]\right\}\rho_{\rm B}(k,t)\right] - \Gamma_d\mu_{5d}(t). \qquad (5)
\end{aligned}
$$

where we take into account the helicity flip of quarks in their collisions by introducing the coefficients $\Gamma_q = e_q^6\mu_q/8\pi^5$ [7].

The quark matter conductivity in Eq. (5) as a function of the matter temperature T has the form [13],

$$
\sigma_{\rm cond} = \sigma_0\frac{T_0^{5/3}}{T^{5/3}}, \quad \sigma_0 = 3.15 \times 10^{22}\,\mathrm{s}^{-1}, \qquad (6)
$$

where $T_0 \sim (10^8 - 10^9)\,\mathrm{K}$ is the typical initial temperature of a thermally relaxed HS/QS. To account for the energy conservation law, we insert the quenching factor,

$$
F_q = 1 - \frac{B^2}{(\mu_u^2+\mu_d^2)T_0^2}, \qquad (7)
$$

in Eq. (5); cf. Ref. [7] and Eq. (6). The quenching factor in Eq. (7) takes into account the dependence of the temperature on the magnetic field [14, 15]: $T^2 = T_0^2 F_q$.

The system in Eq. (5) should be completed with the initial condition. We shall suppose that the initial spectrum of the magnetic energy density has the Kolmogorov form [16],

$$\rho_{\rm B}(k,0) = \mathcal{C}k^{-5/3}, \quad \mathcal{C} = \frac{B_0^2}{3\left(k_{\rm min}^{-2/3} - k_{\rm max}^{-2/3}\right)}, \tag{8}$$

where $k_{\rm min}$ and $k_{\rm max}$ are the minimal and maximal wave numbers and B_0 is the initial magnetic field. For the definiteness we shall take that $k_{\rm max} = 10k_{\rm min}$ and $k_{\rm min}$ will be the free parameter in our model. The initial spectrum of the magnetic field is $h(k,0) = 2\rho_{\rm B}(k,0)/k$, which corresponds to the maximal initial helicity. The initial chiral imbalances are chosen as $\mu_{5u}(0) = \mu_{5d}(0) = 1\,{\rm MeV}$ [7].

If we introduce the dimensionless quantities,

$$\begin{aligned}
\mathcal{H}(\kappa,\tau) = \frac{\alpha_{\rm em}^2}{2\mu_0^2}h(k,t), \quad \mathcal{R}(\kappa,\tau) = \frac{\alpha_{\rm em}^2}{\mu_0^2 k_{\rm min}}\rho_{\rm B}(k,t), \quad \mathcal{M}_{u,d}(\tau) = \frac{\alpha_{\rm em}}{\pi k_{\rm min}}\mu_{5(u,d)}(t), \\
\kappa = \frac{k}{k_{\rm min}}, \quad \tau = \frac{2k_{\rm min}^2}{\sigma_0}t, \quad \mathcal{V}_{u,d} = \frac{\alpha_{\rm em}}{\pi k_{\rm min}}V_{5(u,d)}, \quad \mathcal{G}_{u,d} = \frac{\sigma_0\Gamma_{u,d}}{2k_{\rm min}^2},
\end{aligned} \tag{9}$$

where $\alpha_{\rm em} = e^2/4\pi = 7.3 \times 10^{-3}$ is the fine structure constant, then the system in Eq. (5) can be rewritten in the form,

$$\begin{aligned}
\frac{\partial\mathcal{H}(\kappa,\tau)}{\partial\tau} =& -\kappa^2\left\{F_q^{5/6} + F_q^{-1}K_d\int_1^{\kappa_{\rm max}}{\rm d}\kappa'\mathcal{R}(\kappa',\tau)\right\}\mathcal{H}(\kappa,\tau) \\
&+\left\{0.22F_q^{5/6}\left(4\left[\mathcal{M}_u(\tau)+\mathcal{V}_u\right]+\mathcal{M}_d(\tau)+\mathcal{V}_d\right)\right. \\
&\left.+F_q^{-1}K_d\int_1^{\kappa_{\rm max}}{\rm d}\kappa'\kappa'^2\mathcal{H}(\kappa',\tau)\right\}\mathcal{R}(\kappa,\tau), \\
\frac{\partial\mathcal{R}(\kappa,\tau)}{\partial\tau} =& -\kappa^2\left\{F_q^{5/6} + K_dF_q^{-1}\int_1^{\kappa_{\rm max}}{\rm d}\kappa'\mathcal{R}(\kappa',\tau)\right\}\mathcal{R}(\kappa,\tau) \\
&+\kappa^2\left\{0.22F_q^{5/6}\left(4\left[\mathcal{M}_u(\tau)+\mathcal{V}_u\right]+\mathcal{M}_d(\tau)+\mathcal{V}_d\right)\right. \\
&\left.-F_q^{-1}K_d\int_1^{\kappa_{\rm max}}{\rm d}\kappa'\kappa'^2\mathcal{H}(\kappa',\tau)\right\}\mathcal{H}(\kappa,\tau), \\
\frac{{\rm d}\mathcal{M}_u(\tau)}{{\rm d}\tau} =& 0.92F_q^{5/6}\int_1^{\kappa_{\rm max}}{\rm d}\kappa\big[\kappa^2\mathcal{H}(\kappa,\tau) \\
&-0.22\left(4\left[\mathcal{M}_u(\tau)+\mathcal{V}_u\right]+\mathcal{M}_d(\tau)+\mathcal{V}_d\right)\mathcal{R}(\kappa,\tau)\big] - \mathcal{G}_u\mathcal{M}_u(\tau), \\
\frac{{\rm d}\mathcal{M}_d(\tau)}{{\rm d}\tau} =& 0.15F_q^{5/6}\int_1^{\kappa_{\rm max}}{\rm d}\kappa\big[\kappa^2\mathcal{H}(\kappa,\tau) \\
&-0.22\left(4\left[\mathcal{M}_u(\tau)+\mathcal{V}_u\right]+\mathcal{M}_d(\tau)+\mathcal{V}_d\right)\mathcal{R}(\kappa,\tau)\big] - \mathcal{G}_d\mathcal{M}_d(\tau),
\end{aligned} \tag{10}$$

where $\kappa_{\rm max} = k_{\rm max}/k_{\rm min}$. The quenching factor F_q in Eq. (10) takes the form,

$$F_q = 1 - \frac{1.61 k_{\rm min}^2}{\alpha_{\rm em}^2 T_0^2} \int_1^{\kappa_{\rm max}} {\rm d}\kappa \mathcal{R}(\kappa, \tau). \tag{11}$$

The coefficient in the turbulence terms in Eq. (10) reads,

$$K_d = 1.25 \times 10^2 \frac{\sigma_0 k_{\rm min}^2}{\alpha_{\rm em}^3 T_0^2 \mu_0}. \tag{12}$$

Note that we also take into account the dependence of the temperature on the magnetic field in the turbulence terms by introducing the factor F_q^{-1} there.

3 Numerical solution of the evolution equations

In this section we present the numerical solution of the system in Eq. (10) with the initial conditions chosen in Sec. 2.

In Fig. 1, we show the time evolution of the magnetic field based on the numerical results of Eq. (10) with the initial conditions chosen in Sec. 2. The numerical simulations were made for various initial temperatures and minimal length scales. In all cases we start with the same magnetic field $B_0 = 10^{12}\,{\rm G}$.

One can see in Figs. 1(a)-1(d) that the initial magnetic field experiences the exponential growth driven by the electroweak interaction between quarks since $V_{5q} \neq 0$. After the magnetic field reaches the maximal value, it drops down about one order of magnitude and then the field demonstrates a slow decrease. The appearance of a peak in the profile of the time evolution of the magnetic field is owing to the turbulence effects accounted for in Eqs. (5) and (10).

Let us define the scale of the magnetic field as $\Lambda = 1/k$. Then the effect of the turbulent matter motion is more sizable for small scale magnetic fields corresponding to a great $k_{\rm min}$, as seen in Eq. (12). To highlight this feature, in Fig. 1, we plot the evolution of the magnetic field at the absence of the turbulence, i.e. when $K_d = 0$, shown as dashed lines. In Figs. 1(a) and 1(b), for $1\,{\rm cm} < \Lambda < 10\,{\rm cm}$, as well as Figs. 1(c) and 1(d), for $10\,{\rm cm} < \Lambda < 10^2\,{\rm cm}$, the difference between the turbulent and nonturbulent cases is clearly seen. For the greater scale magnetic field, shown in Figs. 1(e) and 1(f), corresponding to $2.9 \times 10^2\,{\rm cm} < \Lambda < 2.9 \times 10^3\,{\rm cm}$, the evolution of the magnetic field in the turbulent and nonturbulent situations is less distinguishable in a limited time interval.

4 Application for the description of bursts of magnetars

In this section we discuss the implication of the results of the numerical simulations in Sec. 3 for the explanation of the electromagnetic radiation of magnetars.

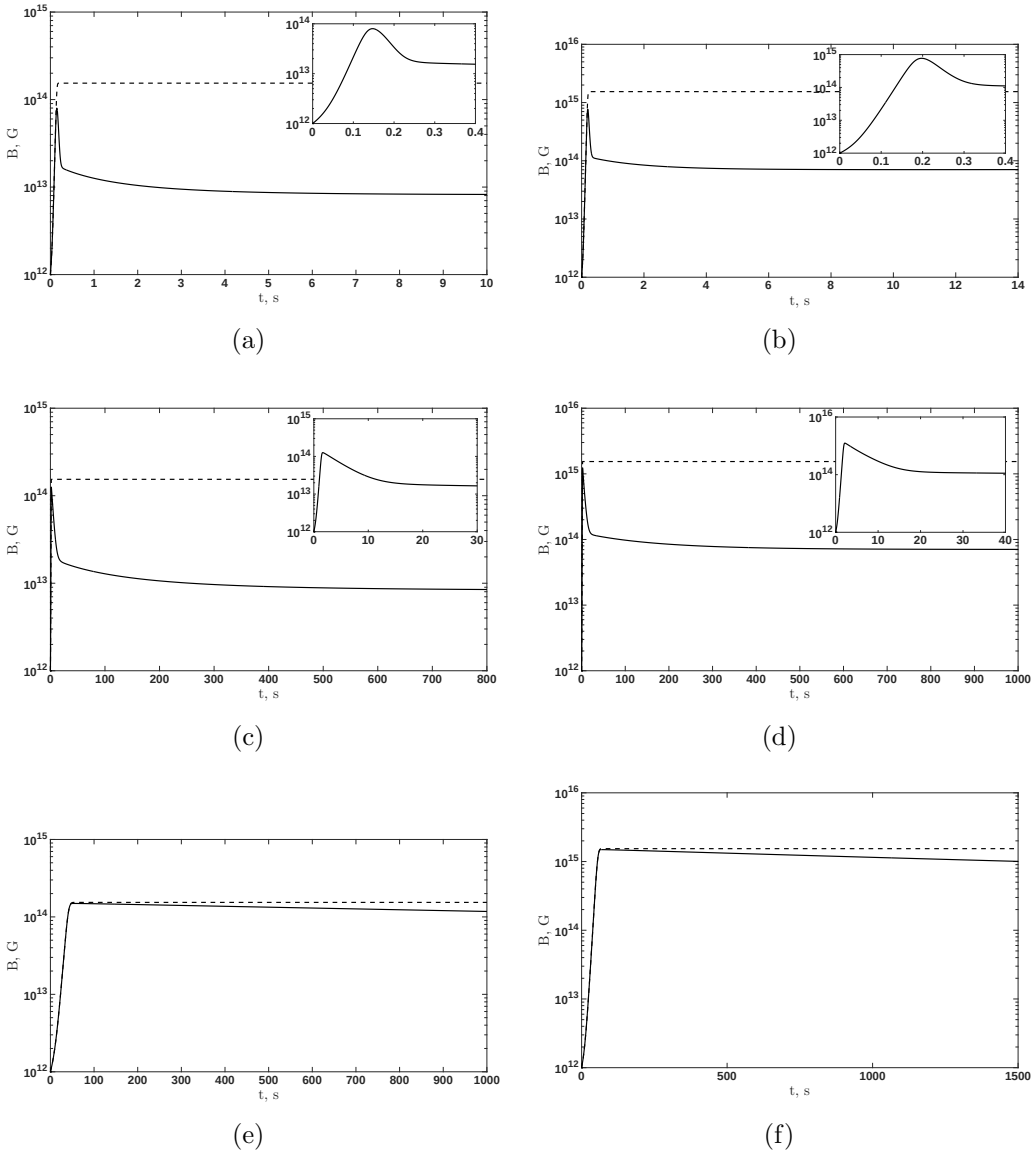

Figure 1: The evolution of the magnetic field for different T_0 and $\Lambda_{\max} = 1/k_{\min}$. The panels (a), (c), and (e) correspond to $T_0 = 10^8$ K, whereas the panels (b), (d), and (f) – to $T_0 = 10^9$ K. The panels (a) and (b) show the evolution of the field with $1\,\mathrm{cm} < \Lambda < 10\,\mathrm{cm}$, the panels (c) and (d) – with $10\,\mathrm{cm} < \Lambda < 10^2\,\mathrm{cm}$, and the panels (e) and (f) – with $2.9 \times 10^2\,\mathrm{cm} < \Lambda < 2.9 \times 10^3\,\mathrm{cm}$. The insets in the panels (a)-(d) demonstrate the magnetic field behavior at small evolution times. Dashed lines represent the magnetic field evolution with the correposding initial conditions at the absence of the turbulence, i.e. when $K_d = 0$.

We mentioned already in Sec. 1 that magnetars are mainly detected by their electromagnetic radiation in the X-ray or soft γ-ray regions as AXP or SGR. This electromagnetic activity is in the form of bursts or flares, which range from short to giant, depending on the duration and the total energy release. In all the events a short peak in the radiation is followed by a slowly decreasing tail. Peaks in short bursts last $\sim 0.1\,\mathrm{s}$ [17] and in giant flares – $\sim (10-20)\,\mathrm{s}$ [18]. The tail of giant flares can be up to $400\,\mathrm{s}$ [18]. Some of the observational data are summarized in Ref. [1].

Nowadays there a lack in understanding of both the origin of the strong magnetic fields in magnetars and the mechanism underlying their bursts and flares. For example, in Ref. [19], it was suggested that the flashes of SGR can be accounted for by the magnetized matter emission through ruptures of the stellar crust in a sort of starquakes. Later another mechanism involving the magnetic energy transmission to the magnetosphere of a magnetar by a thermoplastic wave propagating in a stellar crust was proposed in Ref. [20].

The thermoplastic wave model, which turns out to be the most plausible explanation of magnetar flares now, was further developed in Ref. [21]. It was found in Ref. [21] that the plastic flow becomes irrelevant if $B \lesssim 10^{13}\,\mathrm{G}$. However, the role of the magnetic field in the core of a magnetar is unclear in this model. The quantized vortices and fluxtubes in the superfluid stellar core were suggested in Ref. [21] to play an important role in the thermoplastic wave excitement.

In Ref. [7], we proposed a model for the magnetic field generation in HS/QS based on the magnetic field instability driven by the electroweak interaction of quarks. This model involves the electroweak correction to CME. Note that the existence of quark matter in a compact star is necessary since CME in the presence of the electroweak interaction can take place only if the chiral symmetry is unbroken [23]. Unlike a neutron star, there is a possibility to restore the chiral symmetry in quark matter in HS/QS [24]. In Ref. [7], the amplification of the seed field $B_0 = 10^{12}\,\mathrm{G}$, typical for a pulsar, to $B = (10^{14} - 10^{15})\,\mathrm{G}$, predicted in magnetars [1]. The magnetic fields generated were large scale with $10^2\,\mathrm{m} < \Lambda < 10\,\mathrm{km}$.

Now we are interested in the evolution of smaller scale fields in frames of our model and accounting for the turbulence effects. Let us consider HS/QS in a thermal equilibrium with the initial temperature $T_0 = (10^8 - 10^9)\,\mathrm{K}$. We shall take that the quark matter density $n_0 = 1.8 \times 10^{38}\,\mathrm{cm}^{-3}$, which may well exist in HS/QS. In this case, as results from the numerical simulation in Sec. 3, one can generate the small scale magnetic field with the time behavior resembling very much bursts and flares of magnetars.

Indeed, if we take $T_0 = 10^8\,\mathrm{K}$, the initial pulse of the magnetic field with $B \gtrsim 10^{13}\,\mathrm{G}$ lasts $\sim 0.1\,\mathrm{s}$, see the inset in Fig. 1(a). We recall that the thermoplastic flow is efficient if $B \gtrsim 10^{13}\,\mathrm{G}$ [21]. As mentioned above, such a time interval is typical for a short bursts of magnetars [17]. Then, we can see in the inset in Fig. 1(c) that the duration of the initial pulse of the magnetic field is $\sim (10-15)\,\mathrm{s}$, which is quite close to that one observes in a giant flare in magnetars [18]. The part of the slowly decreasing tail in which $B \gtrsim 10^{13}\,\mathrm{G}$ in Fig. 1(c) lasts $\sim (300-400)\,\mathrm{s}$, which is again quite close to the total duration of a giant flare in magnetars [18]. Even the shape of the initial pulse of the magnetic field obtained in our model is similar to that observed in a giant flare: it has a steeper leading edge and

more slopping tailing edge; cf. the inset in Fig. 1(c) and Ref. [18].

In frames of our model, the magnetic field is generated in a region where the chiral symmetry is unbroken. It appears to happen closer to the stellar core. As mentioned above, the role of the magnetic field in the stellar core is unclear in the thermoplastic wave model [21]. Therefore, if the model in Ref. [21] is valid, the small scale magnetic field predicted in our work could trigger a thermoplastic wave. In this situation the time evolution of the magnetic field resembles very much the bursts and flares in magnetars.

There is an evidence that magnetar flares can be generated by small scale magnetic fields in the stellar core. For example, the initial magnetic field in the magnetar core necessary to induce a short wavelength Hall wave, which then triggers a thermoplastic wave, was found in Ref. [22] to have $\sim 10\,\mathrm{m}$ length scale, which is only one order of magnitude bigger than $\Lambda_{\max}$ used in Sec. 3 to simulate a giant flare; cf. Fig. 1(c). Perhaps 3D simulations announced in Ref. [22] will reveal a closer coincidence with the results of our model.

It is interesting to mention that we can explain the flashes in magnetars ranging from short bursts to giant flares in frames of a single model. The energetics of these events should depend on the wave length of a thermoplastic wave excited. It is reasonable to assume that, if one generates a magnetic field of a larger scale, it will initiate a thermoplastic wave with a larger wave length. It is this feature which results from our simulations: compare Figs. 1(a) and 1(c) as well as Figs. 1(b) and 1(d).

5 Conclusion

In the present work we have studied the evolution of strong magnetic fields in quark matter driven by CME accompanied by the contribution of the electroweak interaction of quarks in Eq. (1). To allow the existence of CME we have assumed that the chiral symmetry in quark matter is unbroken. Since magnetic fields were supposed to be of a relatively small scale, we have accounted for the effects of the turbulent motion of quark matter by simulating the matter velocity with the Lorentz force in Eq. (4). Then we have derived the system of the evolution equations for the spectra on the magnetic helicity density and the magnetic energy density as well as for the chiral imbalances of each type of quarks; cf. Eq. (10). In Sec. 3, this system has been solved numerically with the initial conditions corresponding to HS/QS.

In Sec. 4, we have analyzed the application of the numerically obtained behavior of the magnetic fields for the interpretation of the electromagnetic radiation of AXP and SGR. It has been revealed that, under certain initial conditions, the time evolution of the magnetic field obtained in frames of our model resembles various flashes in magnetars spanning from short bursts to giant flares. Thus small scale magnetic fields generated in the stellar core could trigger the electromagnetic processes in the magnetosphere of a compact star, resulting in the bursts and flares, through, e.g., the mechanism of a thermoplastic wave propagating in the crust of a star, which was recently proposed in Refs. [20, 21]. Hence the mechanism of the magnetic field generation driven by the parity violating electroweak interaction between fermions can be implemented in these compact stars.

Acknowledgements

I am thankful to S.B. Popov and R. Turolla for useful communications, as well as to the Tomsk State University Competitiveness Improvement Program and RFBR (research project No. 15-02-00293).

A Calculation of drag time in degenerate quark matter

In this appendix we shall calculate the drag time $\tau_{\rm D}$, introduced in Sec. 2, due to Coulomb collisions of quarks.

In plasma consisting of u and d quarks, there are three types of collisions: $ud \to ud$, $uu \to uu$, and $dd \to dd$. Let us, first, consider the $ud \to ud$ reaction. The matrix element has the form,

$$\mathcal{M}_{ud} = \frac{\mathrm{i}e_u e_d}{t}\bar{u}(p_1')\gamma^\mu u(p_1)\cdot\bar{d}(p_2')\gamma_\mu d(p_2), \tag{13}$$

where $t = (p_1' - p_1)^2$ is the Mandelstam variable, $u(p)$ and $d(p)$ are the bispinors of u and d quarks corresponding to the initial $p_{1,2}$ and final $p_{1,2}'$ momenta, and $\gamma^\mu = (\gamma^0, \boldsymbol{\gamma})$ are the Dirac matrices. The matrix element squared takes the form,

$$|\mathcal{M}_{ud}|^2 = \frac{e_u^2 e_d^2}{t^2}\mathrm{tr}\left(\rho_2'\gamma_\mu\rho_2\gamma_\nu\right)\cdot\mathrm{tr}\left(\rho_1'\gamma^\mu\rho_1\gamma^\nu\right), \tag{14}$$

where

$$\rho_{1,2} = \frac{1}{2}\gamma_\mu p_{1,2}^\mu\left(1 - \chi_{1,2}\gamma^5\right), \quad \rho_{1,2}' = \frac{1}{2}\gamma_\mu p_{1,2}'^\mu, \tag{15}$$

are the spin density matrices for the initial and final quark states [25, p. 111]. Here $\chi = \pm 1$ is the helicity of the initial quarks ($\chi = +1$ for right quarks and $\chi = -1$ for left particles) and $\gamma^5 = \mathrm{i}\gamma^0\gamma^1\gamma^2\gamma^3$. Eq. (15) implies that we assume unpolarized final states. Using Eq. (15), one can transform Eq. (14) to the form,

$$|\mathcal{M}_{ud}|^2 = \frac{e_u^2 e_d^2}{2t^2}\left[s^2 + u^2 + \chi_1\chi_2\left(s^2 - u^2\right)\right], \tag{16}$$

where $s = (p_1 + p_2)^2$ and $u = (p_1 - p_2')^2$ are the Mandelstam variables.

The total probability of the ud scattering per unit time reads

$$W_{ud} = 2\left(W_+ + W_-\right), \quad W_+ = \frac{V e_u^2 e_d^2}{4(2\pi)^8}\left\langle\frac{s^2}{t^2}\right\rangle, \quad W_- = \frac{V e_u^2 e_d^2}{4(2\pi)^8}\left\langle\frac{u^2}{t^2}\right\rangle, \tag{17}$$

where V is the normalization volume and the averaging of a variable $X = X(p_1, \ldots, p_2')$ is defined as

$$\begin{aligned}\langle X\rangle = \int \frac{\mathrm{d}^3p_1\mathrm{d}^3p_2\mathrm{d}^3p_1'\mathrm{d}^3p_2'}{E_1E_2E_1'E_2'}X\delta^4(p_1 + p_2 - p_1' - p_2') \\ \times f(E_1 - \mu_u)\left[1 - f(E_1' - \mu_u)\right]f(E_2 - \mu_d)\left[1 - f(E_2' - \mu_d)\right].\end{aligned} \tag{18}$$

Here $E = |\mathbf{p}|$ is the energy of a massless quark, $f(E) = [\exp(\beta E) + 1]^{-1}$ is the Fermi-Dirac distribution function, $\beta = 1/T$ is the reciprocal temperature, and $\mu_{u,d}$ are the chemical potentials of u and d quarks. Note that $W_{\pm}$ in Eq. (17) correspond to $\chi_1\chi_2 = \pm 1$ in Eq. (16). In Eq. (16) we take into account all possible initial helicities and sum over the polarization states of the outgoing quarks.

Let us first compute $\langle s^2/t^2 \rangle$. After that integration over $\mathbf{p}_2'$ with help of the momentum conservation delta function, Eq. (18) takes the form,

$$\left\langle \frac{s^2}{t^2} \right\rangle = \int \frac{\mathrm{d}^3p_1 \mathrm{d}^3p_1' \mathrm{d}^3p_2}{E_1E_2E_1'E_2'} \frac{\left[E_1E_2 - (\mathbf{p}_1 \cdot \mathbf{p}_2)\right]^2}{\left[E_1E_1' - (\mathbf{p}_1 \cdot \mathbf{p}_1')\right]^2} \delta(E_1 + E_2 - E_1' - E_2') \\ \times f(E_1 - \mu_u)\left[1 - f(E_1' - \mu_u)\right] f(E_2 - \mu_d)\left[1 - f(E_2' - \mu_d)\right], \tag{19}$$

where $E_2' = |\mathbf{q} - \mathbf{p}_2|$ and $\mathbf{q} = \mathbf{p}_1' - \mathbf{p}_1$. Then we represent $\mathrm{d}^3p_2 = E_2^2 \mathrm{d}E_2 \mathrm{d}\cos\theta \mathrm{d}\varphi$ in Eq. (19) and choose the geometry as shown in Fig. 2. In this case $(\mathbf{p}_1 \cdot \mathbf{p}_2) = E_1E_2(\cos\theta\cos\theta_1 + \sin\theta\sin\theta_1\cos\varphi)$ and

$$\delta(E_1 + E_2 - E_1' - E_2') = \frac{E_2'}{qE_2}\delta(\cos\theta - \cos\theta_0), \quad \cos\theta_0 \approx \cos\theta_1 + \frac{q}{2E_2}\sin^2\theta_1\left(1 + \frac{E_2}{E_1}\right). \tag{20}$$

Moreover, taking into account that the quark matter is highly degenerate, one gets that $f(E_{1,2} - \mu_{u,d})\left[1 - f(E_{1,2}' - \mu_{u,d})\right] \approx T\delta(E_{1,2} - \mu_{u,d})$. Finally, after the integration over $\mathbf{p}_2'$, Eq. (19) is transformed to

$$\left\langle \frac{s^2}{t^2} \right\rangle = 6\pi T^2\mu_d^2 \int \mathrm{d}^3p_1 \mathrm{d}^3p_1' \frac{\sin^4\theta_1 \delta(E_1 - \mu_u)}{q\left[E_1E_1' - (\mathbf{p}_1 \cdot \mathbf{p}_1')\right]^2}. \tag{21}$$

Eq. (21) can be further simplified if we change the integration variable $\mathbf{p}_1' \to \mathbf{q} = \mathbf{p}_1' - \mathbf{p}_1$ and notice that $E_1E_1' - (\mathbf{p}_1 \cdot \mathbf{p}_1') \approx (q^2/2)\sin^2\theta_1$. Eventually we obtain that

$$\left\langle \frac{s^2}{t^2} \right\rangle = 192\pi^3T^2\mu_d^2\mu_u^2 \int_0^{\infty} \frac{\mathrm{d}q}{\left(q^2 + \omega_p^2\right)^{3/2}} = 192\pi^3\mu_d^2\mu_u^2\frac{T^2}{\omega_p^2}, \tag{22}$$

where we introduce the plasma frequency in the degenerate ud matter [7, 26],

$$\omega_p = \frac{1}{\sqrt{3}\pi}\sqrt{e_u^2\mu_u^2 + e_d^2\mu_d^2}, \tag{23}$$

to avoid the infrared divergence in Eq. (22).

Analogously one can compute W_-. The direct calculation shows that $W_- = W_+$. It gives one the total probability of the ud scattering in the form,

$$W_{ud} = \frac{9V}{4\pi^3}\frac{e_u^2e_d^2\mu_d^2\mu_u^2}{e_u^2\mu_u^2 + e_d^2\mu_d^2}, \tag{24}$$

where we use Eqs. (17), (22), and (23).

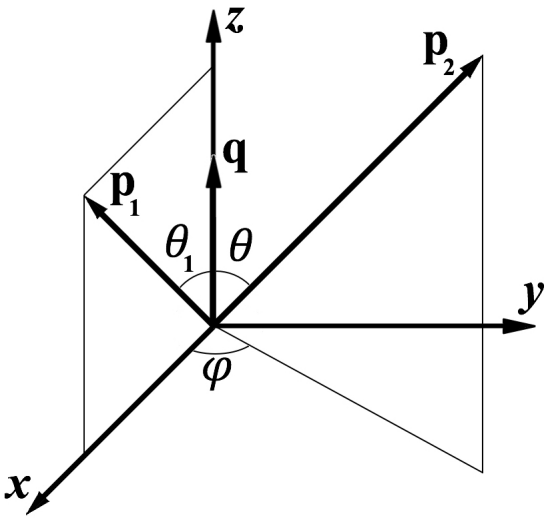

Figure 2: The geometry for the integration over $\mathbf{p}_1$ and $\mathbf{p}_2$.

Now let us consider the scattering of identical quarks, e.g. the $uu \to uu$ reaction. The matrix element of this process is

$$\mathcal{M}_{uu} = \mathrm{i}e_u^2 \left[\frac{1}{t} \bar{u}(p_1')\gamma^\mu u(p_1) \cdot \bar{u}(p_2')\gamma_\mu u(p_2) - \frac{1}{u} \bar{u}(p_2')\gamma^\mu u(p_1) \cdot \bar{u}(p_1')\gamma_\mu u(p_2) \right]. \tag{25}$$

The matrix element in Eq. (25) squared takes the form [25, p. 327],

$$|\mathcal{M}_{uu}|^2 = \frac{e_u^4}{2} \left[\frac{s^2+u^2}{t^2} + \frac{s^2+t^2}{u^2} + \chi_1\chi_2 \left(\frac{s^2-u^2}{t^2} + \frac{s^2-t^2}{u^2} \right) \right]. \tag{26}$$

Performing similar calculations as in the ud case and using Eq. (26), one obtains the total probability of the $uu \to uu$ reaction as

$$W_{uu} = \frac{9V}{2\pi^3} \frac{e_u^4 \mu_u^4}{e_u^2\mu_u^2 + e_d^2\mu_d^2} \left\{ 1 + \frac{2}{3}\frac{\omega_p^2}{\mu_u^2} \left[\ln\left(\frac{\mu_u}{\sqrt{2}\omega_p} \right) + 1 \right] \right\}. \tag{27}$$

The expression for the total probability of the $dd \to dd$ scattering W_{dd} can be obtained on the basis of Eq. (27) by replacing $e_u \to e_d$ and $\mu_u \to \mu_d$.

Let us define the drag time as

$$\tau_\mathrm{D} = \frac{N_u}{W_{uu}} + \frac{N_d}{W_{dd}} + \frac{\sqrt{N_u N_d}}{W_{ud}}, \tag{28}$$

where $N_{u,d} = n_{u,d}V$ are the total densities of u and d quarks and $n_{u,d}$ are the corresponding number densities. Using Eqs. (24) and (27) we obtain the following expression for τ_D:

$$\tau_\mathrm{D} = \frac{4\pi}{27T^2} \left(e_u^2\mu_u^2 + e_d^2\mu_d^2 \right) \left(\frac{2}{e_u^4\mu_u} + \frac{2}{e_d^4\mu_d} + \frac{2}{e_u^2 e_d^2 \sqrt{\mu_u\mu_d}} \right), \tag{29}$$

where we keep only the leading term. Finally, using the values of e_q and μ_q in Sec. 2, one gets for $\tau_{\rm D}$

$$\tau_{\rm D} = 2.5 \frac{\mu_0}{\alpha_{\rm em} T^2}, \tag{30}$$

which will be used in Sec. 2. It should be noted that the dependence of $\tau_{\rm D}$ in Eq. (30) on $\alpha_{\rm em}$ and T coincides with that found in Ref. [27], where collisions between electrons and protons in degenerate matter were studied.

References

[1] R. Turolla, S. Zane, A.L. Watts, Magnetars: the physics behind observations. A review, Rep. Prog. Phys. **78** (2015) 116901, arXiv:1507.02924.

[2] V.A. Miransky, I.A. Shovkovy, Quantum field theory in a magnetic field: From quantum chromodynamics to graphene and Dirac semimetals, Phys. Rept. **576** (2015) 1–209, arXiv:1503.00732.

[3] C. Wang, D. Lai, J. Han, Neutron star kicks in isolated and binary pulsars: Observational constraints and implications for kick mechanisms, Astrophys. J. **639** (2006) 1007–1017, astro-ph/0509484.

[4] D.E. Kharzeev, Topology, magnetic field, and strongly interacting matter, Annu. Rev. Nucl. Part. Sci. **65** (2015) 193–214, arXiv:1501.01336.

[5] M. Dvornikov, V.B. Semikoz, Magnetic field instability in a neutron star driven by the electroweak electron-nucleon interaction versus the chiral magnetic effect, Phys. Rev. D **91** (2015) 061301, arXiv:1410.6676.

[6] A. Boyarsky, O. Ruchayskiy, M. Shaposhnikov, Long-range magnetic fields in the ground state of the Standard Model plasma, Phys. Rev. Lett. **109** (2012) 111602, arXiv:1204.3604.

[7] M. Dvornikov, Generation of strong magnetic fields in dense quark matter driven by the electroweak interaction of quarks, Nucl. Phys. B **913** (2016) 79–92, arXiv:1608.04946.

[8] N.K. Glendenning, Compact Stars: Nuclear Physics, Particle Physics, and General Relativity, 2nd ed., Springer, New York, 2000, pp. 337–362 and 414–440.

[9] M. Dvornikov, V.B. Semikoz, The influence of the turbulent motion on the chiral magnetic effect in the early universe, arXiv:1612.05897.

[10] M. Dvornikov, Galvano-rotational effect induced by electroweak interactions in pulsars, J. Cosmol. Astropart. Phys. 05 (2015) 037, arXiv:1503.00608.

[11] G. Sigl, Cosmological magnetic fields from primordial helical seeds, Phys. Rev D. **66** (2002) 123002, astro-ph/0202424.

[12] J.M. Cornwall, Speculations on primordial magnetic helicity, Phys. Rev. D **56** (1997) 6146–6154, hep-th/9704022.

[13] H. Heiselberg, C.J. Pethick, Transport and relaxation in degenerate quark plasmas, Phys. Rev. D **48** (1993) 2916–2928.

[14] M. Dvornikov, Relaxation of the chiral imbalance and the generation of magnetic fields in magnetars, J. Exp. Theor. Phys. **123** (2016) 967–978 [Zh. Eksp. Teor. Fiz. **150** (2016) 1113–1126], arXiv:1510.06228.

[15] M. Dvornikov, Relaxation of the chiral chemical potential in dense matter of a neutron star, to be published in Russ. Phys. J. (2017) [Izv. Vuz. Fiz. **59** (2016) 132–140].

[16] M. Dvornikov, V.B. Semikoz, Energy source for the magnetic field growth in magnetars driven by the electron-nucleon interaction, Phys. Rev. D **92** (2015) 083007, arXiv:1507.03948.

[17] D. Huppenkothen, et al., Quasi-periodic oscillations and broadband variability in short magnetar bursts, Astrophys. J. **768** (2013) 87, arXiv:1212.1011.

[18] M. Feroci, et al., The giant flare of 1998 August 27 from SGR 1900+14. I. An interpretive study of BeppoSAX and Ulysses observations, Astrophys. J. **549** (2001) 1021–1038, astro-ph/0010494.

[19] R. Perna, J.A. Pons, A unified model of the magnetar and radio pulsar bursting phenomenology, Astrophys. J. Lett. **727** (2011) L51, arXiv:1101.1098.

[20] A.M. Beloborodov, Yu. Levin, Thermoplastic waves in magnetars, Astrophys. J. Lett. **794** (2014) L24, arXiv:1406.4850.

[21] S.K. Lander, Magnetar field evolution and crustal plasticity, Astrophys. J. Lett. **824** (2016) L21, arXiv:1604.02972.

[22] X. Li, Yu. Levin, A.M. Beloborodov, Magnetar outbursts from avalanches of Hall waves and crustal failures, Astrophys. J. **833** (2016) 189, arXiv:1606.04895.

[23] M. Dvornikov, Role of particle masses in the magnetic field generation driven by the parity violating interaction, Phys. Lett. B **760** (2016) 406–410, arXiv:1608.04940.

[24] M. Buballa, S. Carignano, Inhomogeneous chiral symmetry breaking in dense neutron-star matter, Eur. Phys. J. A **52** (2016) 57–72, arXiv:1508.04361.

[25] V.B. Berestetskii, E.M. Lifschitz, L.P. Pitaevskii, Quantum Electrodynamics, 2nd ed., Pergamon, Oxford, 1982.

[26] E. Braaten, D. Segel, Neutrino energy loss from the plasma process at all temperatures and densities, Phys. Rev. D **48** (1993) 1478–1491, hep-ph/9302213.

[27] D.C. Kelly, Electrical and thermal conductivities of a relativistic degenerate plasma, Astrophys. J. **179** (1973) 599–606.